Polymorphism of Ca^{2+} Sparks Evoked from In-Focus Ca^{2+} Release Units in Cardiac Myocytes

Jian-Xin Shen,*† ShiQiang Wang,†‡ Long-Sheng Song,† Taizhen Han,* and Heping Cheng†‡
*Department of Physiology, Medical School of Xi'an Jiaotong University, Xi'an 710061, China; †Laboratory of Cardiovascular Science, National Institute on Aging, National Institutes of Health, Baltimore, Maryland 21224; and ‡National Laboratory of Biomembrane and Membrane Biotechnology, College of Life Science, Peking University, Beijing, China

ABSTRACT Ca^{2+} sparks are the elementary release events in many types of cells. Here we present a morphometric analysis of Ca^{2+} sparks (i.e., amplitude and kinetic parameters) using an approach that minimizes the confounding factor of the detection of out-of-focus events. By activation and visualization of Ca^{2+} sparks from Ca^{2+} release units under loose-seal patch-clamp conditions, we found that the amplitude and rising rate of in-focus sparks exhibited a broad modal distribution, whereas spark rise time and spatial width appeared to be stereotyped. Spark morphometrics were constant irrespective of the latency of spark production and the time-dependent L-type Ca^{2+} channel activation. Polymorphism of Ca^{2+} sparks in terms of variable amplitude and rising rate was evident for events from the same release units, and intra- and interrelease unit variability contributed equally to the overall variability. The rising rate, a reporter of the underlying Ca^{2+} release flux, displayed a strong positive correlation with spark amplitude, but a negative correlation with spark rise time, an index of Ca^{2+} release duration. On the basis of Ca^{2+} spark morphometrics measured here, we suggested a model in which cohorts of variable number of ryanodine receptors are activated in the genesis of Ca^{2+} sparks, and the ensuing negative feedback overrides the regenerative Ca^{2+}-induced Ca^{2+} release to extinguish the ongoing Ca^{2+} spark.

INTRODUCTION

Ca^{2+} sparks are microscopic, short-lived Ca^{2+} release events that are mediated by the ryanodine receptor (RyR)/Ca^{2+} release channels in the endoplasmic and sarcoplasmic reticulum (SR). Discovered in heart cells, Ca^{2+} sparks have been found in many types of excitable and nonexcitable cells, and are thought to constitute the elementary units of intracellular Ca^{2+} signaling in heart (Cheng et al., 1993; Cannell et al., 1995; Lipp and Niggli, 1994; Lopez-Lopez et al., 1995), brain (Haak et al., 2001), skeletal, and smooth muscle (Klein et al., 1996; Nelson et al., 1995; Tsugorka et al., 1995). Over the last decade, extensive studies have focused on morphometrics or anatomy of Ca^{2+} sparks (as visualized by confocal fluorescent microscopy), which are essential to elucidation of the exact nature of Ca^{2+} sparks and delineation of the spatial and temporal scope of spark-driven local Ca^{2+} signaling. Ironically, intrinsic properties of Ca^{2+} sparks continue to be a matter of debate. A major confounding factor is that Ca^{2+} sparks usually occur at random locations in relation to the focal volume under observation. As a result, those at out-of-focus positions will display reduced amplitude, broadened spatial spreading, and blunted kinetics, with the degree of distortion depending on the distance from the confocal volume (Pratusevich and Balke, 1996; Smith et al., 1998). Indeed, both confocal sampling theory and experiments aided with an automated spark detection algorithm have shown that the apparent spark amplitude always obeys a monotonically decaying distribution (modified by the detectability function), regardless of the true spark amplitude (Cheng et al., 1999).

Several approaches have been developed to curtail or correct for the effects of optical blurring on certain aspects of Ca^{2+} spark properties. In an effort to restore true population statistics of spark amplitude, Izu et al. and Rios et al. have attempted to deconvolve the optical blurring from the apparent spark amplitude distribution (Izu et al., 1998; Rios et al., 2001). We measured the release duration of Ca^{2+} sparks when it became relatively insensitive to optical blurring by limiting Ca^{2+} sparks in space and time with a nonfluorescent, slow Ca^{2+} buffer (Wang et al., 2002). Many investigators have exploited spark repeats from fixed release units that underwent an unusual, high-frequency spontaneous activity to analyze the variability in spark amplitude (Klein et al., 1999; Wang et al., 2002). Spark variability has also been analyzed using cardiac Ca^{2+} sparks that were evoked by repeated action potentials in the presence of a reduced external Ca^{2+} (0.5 mmol/L) at fixed T-tubule-SR junctions (Bridge et al., 1999). Notwithstanding limitations, information gleaned from these studies suggested that Ca^{2+} sparks are rather stereotypic by virtue of modal amplitude distribution or preferred release duration (Bridge et al., 1999; Izu et al., 1998; Klein et al., 1999; Rios et al., 2001; Wang et al., 2002). These impose important constraints on the possible mechanism underlying the genesis of Ca^{2+} sparks. For instance, it has been argued that the rise time characteristics are incompatible with the idea that a spark arises from a single-channel RyR with a reversible Markovian gating scheme. Rather, Ca^{2+} sparks either are a collective phenomenon of a group of interacting RyRs or originate from single RyRs that manifest a rare,

Submitted July 10, 2003, and accepted for publication September 11, 2003.
Address reprint requests to Heping Cheng, PhD, Laboratory of Cardiovascular Science, National Institute on Aging, NIH, 5600 Nathan Shock Dr., Baltimore, MD 21224. Tel.: 410-558-8634; Fax: 410-558-8150; E-mail: chengp@grc.nia.nih.gov.

0006-3495/04/01/182/09 $2.00

thermodynamically irreversible gating (Shirokova et al., 1999; Wang et al., 2002).

Recently we have developed the loose-seal patch-clamp and confocal imaging technique by which one can visualize in-focus sparks triggered by single L-type Ca^{2+} channel (LCC) currents in intact cardiac myocytes (Wang et al., 2001), via the Ca^{2+}-induced Ca^{2+} release (CICR) mechanism (Fabiato, 1985). Naturally, this approach eliminates the out-of-focus events; in-focus detection of sparks against a quiescent background further enhances the spark detectability. In contrast to the notion that sparks are stereotypical, a broad modal amplitude distribution was reported (Wang et al., 2001), hinting on polymorphism of Ca^{2+} sparks in appearance and origin.

Using this newly developed technique, here we intended to characterize systematically main aspects of spark morphometrics, including amplitude, rise time, spatial width, and rising rate, and to analyze their intrinsic variability as well as interrelationship, under physiological experimental conditions. Our results confirmed a rather synchronized spark rise time, demonstrated a stereotyped spatial width, but uncovered a substantial variability in spark amplitude and mean rising rate. The polymorphism of Ca^{2+} sparks suggests that spark genesis involves stochastic activation of variable numbers of RyRs. In addition, an inverse relationship between spark rise time and rising rate provides evidence for a negative feedback mechanism in the regulation of termination of Ca^{2+} sparks.

METHODS

Cell isolation

Ventricular myocytes were isolated from adult Sprague-Dawley rats (age, 2–3 months; weight, 225–300 g) by using a standard enzymatic technique, as described previously (Song et al., 2001). Briefly, after anesthesia (sodium pentobarbitone, 100 mg kg^{-1} injected I.P.), the heart was removed from the chest and perfused retrogradely via the aorta using the Langendorff method and collagenase (Worthington type II, 1 mg ml^{-1}). Single cells were shaken loose from the heart, minced after this perfusion procedure, in HEPES buffer solution containing (in mmol/L): 137 NaCl, 5.4 KCl, 1.2 $MgCl_2$, 1.2 NaH_2PO_4, 1 $CaCl_2$, 10 glucose, and 20 HEPES (pH 7.4 adjusted with NaOH).

Confocal Ca^{2+} imaging

Isolated single myocytes were first incubated with the Ca^{2+} indicator fluo-4-AM (15 μM) (Molecular Probes, Eugene, OR) for 5 min, followed by a 10-min rest allowing for de-esterfication of the indicator. The criteria for cell selection included rod shape, clear striation, crisp and clean cell surface, and lack of spontaneous contractions during a 1-min observation period. Confocal imaging was performed using a Zeiss LSM510 confocal microscope (Carl Zeiss Inc., Oberkochen, Germany) equipped with an argon laser (488 nm) and a 40×, 1.3 NA oil immersion objective, at axial and radial resolutions of 1.0 and 0.4 μm, respectively. An *x-z* section image across the pipette tip was first taken to guide the positioning of the focal plane such that half of the rim of the pipette tip (at ~45° angle to the horizontal plane) was discernible. Then, fast *x-y* imaging was performed at a rate of 16 ms per frame, or linescan (*x-t*) imaging was performed with space-time sampling rates of 0.77 ms per scan line and 0.045 μm per pixel.

Loose-seal patch clamp

Cell-attached patch clamping was established using axopatch 200B amplifier (Axon Instruments, Foster City, CA) in loose-seal configuration, as described previously (Wang et al., 2001). A glass pipette (5–7 MΩ, <1 μm at the tip) was gently pressed onto the cell surface to form a low-resistance seal (20–40 MΩ). The patch membrane voltage was determined according to the equation $V_{PM} = RP - V_{com}R_s/(R_s + R_p)$, where V_{PM} refers to the patch membrane voltage, RP the resting potentials (-80.6 ± 7.0 mV, $n = 8$, measured in separate experiments), V_{com} the command voltage applied, R_s and R_p the seal and pipette resistance, respectively. The extracellular and patch pipette filling solution contained (in mmol/L): 137 NaCl, 1 $CaCl_2$, 4.9 KCl, 1 $MgCl_2$, 1.2 NaH_2PO_4, 15 glucose, and 20 HEPES (pH 7.4 adjusted with NaOH). All experiments were done at room temperature (23–25°C), with the V_{PM} at −10 mV or more negative.

Image data analysis

Ca^{2+} Spark detection algorithm was described previously (Cheng et al., 1999), with some minor modifications. Computer programs for the automated spark detection and measurement were coded with IDL software (Research Systems, Boulder, CO). The detectability and rate of false detection under current parameter settings and signal-to-noise characteristics were assessed with an averaged spark embedded in pixel-scrambled blank images (see text). Ca^{2+} spark amplitudes are usually measured as $\Delta R = \Delta F/F_0$, where F_0 refers to the background fluo-4 signal. The rise time was measured as the temporal interval between the takeoff (i.e., ΔF first exceeds 2× standard deviation of the baseline) and the peak of the spark. The maximal rising rate was computed by differentiation of local Ca^{2+} transient using 3-point Langrangian interpolation after minimal smoothing. The mean rising rate was determined as the peak $\Delta F/F_0$ divided by the corresponding rise time.

Statistical analysis

Data were shown as mean ± SD, if not otherwise specified. Nonparametric Kruskal-Wallis test was applied to appraise difference between means of spark parameters. A p-value less than 0.05 was considered statistically significant.

RESULTS

Activation and visualization of Ca^{2+} sparks from in-focus release sites

To investigate intrinsic properties of Ca^{2+} sparks, we adopted the loose-seal patch-clamp and confocal imaging approach (Wang et al., 2001) to image SR Ca^{2+} release from a defined in-focus volume of cytoplasm. Specifically, a glass pipette (<1 μm at the tip) was gently pressed onto the cell surface to form a 20–40-MΩ seal while retaining the integrity of the coupling between sarcolemmal LCCs and RyRs in the SR. This loose-seal configuration enables voltage control of the membrane delimited by the tip of the patch pipette and permits voltage-dependent activation of the LCCs therein, but precludes simultaneous recording of LCC single-channel currents due to excessive electrical noise (Wang et al., 2001). To visualize locally evoked SR Ca^{2+} release events, confocal imaging of the Ca^{2+}-sensitive fluo-4 fluorescence was performed with the focal plane placed right beneath the patch membrane.

Fig. 1 *A* shows representative confocal *x-y* imaging of local Ca^{2+} dynamics underneath the loose-seal patch in an intact rat ventricular myocyte. The confocal plane was positioned such that half of the rim of the patch pipette (at 45° angle of the horizontal plane) was visible. Patch membrane depolarization to ~−25 mV for 300 ms elicited a solitary Ca^{2+} spark, which originated from a focal point beneath the patch membrane. Fast two-dimensional (*x-y*) imaging (16 ms per frame) revealed that, during its evolution, the evoked spark remained spatially confined, without igniting other spark-generating sites. This demonstrates that the current approach allows for investigation of Ca^{2+} sparks from a single in-focus release unit.

To better resolve unitary properties of evoked Ca^{2+} sparks, data were routinely collected in the linescan (*x-t*) imaging mode at a high spatiotemporal resolution (Fig. 2 *A*). Under our experimental conditions (1 mmol/L extracellular Ca^{2+}, no LCC agonist included), direct contribution of the trigger LCC Ca^{2+} influx to an evoked Ca^{2+} spark should be negligible (i_{Ca} ~0.12 pA lasting ~1 ms at −25 mV) (Guia et al., 2001). To ensure single-release unit origin of sparks in individual patches, we further determined mass centers for events collected from the same patch (Fig. 2 *A*). Ca^{2+} sparks originated from different release sites should be projected onto different locations on the scan line, unless they are on the same vertical (*z*) axis. Those patches with spark mass centers wandering over a distance greater than 0.4 μm (4 out of 31 patches) were rejected without further analysis. Otherwise, all active patches ($n = 27$) bearing one or more evoked Ca^{2+} sparks were included for statistical analysis. Among them, a total of 166 Ca^{2+} sparks, excluding a few reactivating events, were activated in 215 voltage pulses

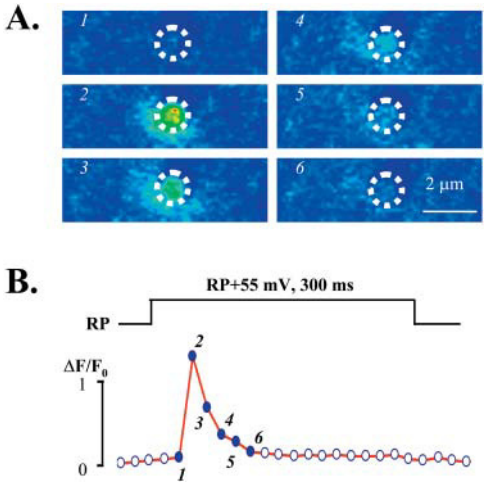

FIGURE 1 Fast *x-y* imaging of an evoked Ca^{2+} spark beneath a loose-seal patch. (*A*) Six sequential confocal images taken at 16-ms intervals during depolarization from resting potential (*RP*, −80 mV) to *RP* + 55 mV. The dashed circle denotes the rim of the pipette. (*B*) Time course of local Ca^{2+} transient. The numbers mark the time points corresponding to the images in *A*. Similar results were obtained in five different patches.

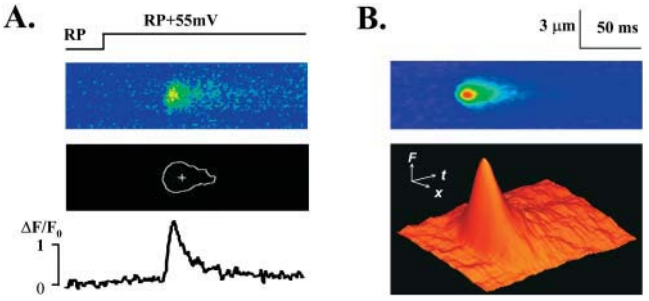

FIGURE 2 Measurement of Ca^{2+} sparks elicited by loose-seal patch depolarization. (*A*) A typical example. From top to bottom: the voltage protocol, linescan image of the evoked spark, its contour plot at $\Delta F/F_0 = 0.25$ and its mass center (marked by the *cross*), and time course of local Ca^{2+} transient (spatially averaged over 1.1-μm width). The mass center coordinates (X, T) were determined by $X = \int\int x\Delta F\,dx\,dt / \int\int DF\,dx\,dt$ and $T = \int\int t\Delta F\,dx\,dt / \int\int DF\,dx\,dt$. (*B*) Space-time characteristics of a spark averaged from 11 unequivocal events. Note that the pipette rim artifact in Fig. 1 was large removed in the pseudoratio (F/F_0) image.

beneath the pipette (i.e., in the image strips of 2 μm × 300 ms). The null event rate was 49 out of 215 pulses (69 null events in the first 200 ms), and the spark activation probability in a single unit during 300-ms depolarization to ~−25 mV was therefore 0.77 for 300-ms depolarization or 0.68 for 200-ms depolarization. The average latency for spark activation, defined as the time lapsed since the onset of depolarization, was 51 ± 46 ms ($n = 147$ sparks) for events in the first 200-ms period. When Ca^{2+} ''spike'' at a T-tubule-SR junction (Song et al., 2001) are mostly single-spark events (e.g., at low voltages under whole-cell voltage-clamp conditions), their activation latency should be the same as that of loose-seal triggered sparks. To this end, the latency reported for spike activation in 200 ms pulses is 70 or 45 ms at −30 or −20 mV, respectively (Song et al., 2001). Thus, the similarity in kinetics of spark and spike activation at around −25 mV provides a validation that local CICR remains largely intact under our experimental conditions. Moreover, since the rate of occurrence of spontaneous Ca^{2+} sparks is typically 1.0 event per second per 100-μm scan in intact cells (Cheng et al., 1996, 1993), contribution of spontaneous spark activity from adjacent sites to the defined volume of observation during depolarization would also be minimal (1%).

Assessment of detectability and false detection

Detection of Ca^{2+} sparks amidst noise is subjected to two types of errors, the rejection of small events (false negatives) and the erroneous detection of noise as spark events (false positives) (Cheng et al., 1999). Evidently, both false positives and false negatives will not only distort the population statistics, but also affect the analysis of variability of spark morphometric parameters. In this study, in-focus activation of sparks against quiescent backgrounds should

improve the detection of low-amplitude events. Moreover, owing to the superior signal-to-noise characteristics afforded by current generation of confocal microscope, we expected a low rate of false detection. To appraise quantitatively the detectability and false detection, we generated a spark test standard by averaging 11 unequivocal events (Fig. 2 *B*) and constructed noise backgrounds based on pixel scrambling of null images. By scaling and embedding the test spark in the noise background, we then fed test images through the same algorithm for spark detection. We found that the detectability was 7.5, 25, or 59% at 0.10, 0.125, or 0.15 in $\Delta F/F_0$ unit, respectively, and reached nearly unity at 0.20 $\Delta F/F_0$ units (Fig. 3, *left*), with the 50% cutoff level at around 0.15 $\Delta F/F_0$ units. There were seven false positives detected in 100 blank images (512 × 512 pixels), so we estimated about one false positive in 215 image strips of 2 μm × 300 ms. Given that the smallest spark events detected by the loose-seal technique was of 0.27 $\Delta F/F_0$ units (see Fig. 4 *B*), these indicate that virtually all local Ca^{2+} release events could be detected with little contamination of false positives under our experimental conditions, providing no subspark release events (Lipp and Niggli, 1996, 1998) substantially smaller than 0.15 $\Delta F/F_0$ units. The high spark detectability and low rate of false detection were made possible, in part, because of the superior signal-to-noise characteristics of contemporary confocal microscopy. In blank traces the background fluctuation of fluo-4 signal was equivalent to merely 0.05 $\Delta F/F_0$ units, and the peak noise level was 0.14 ± 0.03 $\Delta F/F_0$ units ($n = 21$) (Fig. 3, *right*). Since spark detection used multiple cues rather than relying solely on peak amplitude, we were able to detect test events with amplitudes smaller than the peak noise (Fig. 3, *left*). Collectively, these improvements enabled us to depict true spark properties and their intrinsic variability with unprecedented accuracy under well-controlled experimental conditions.

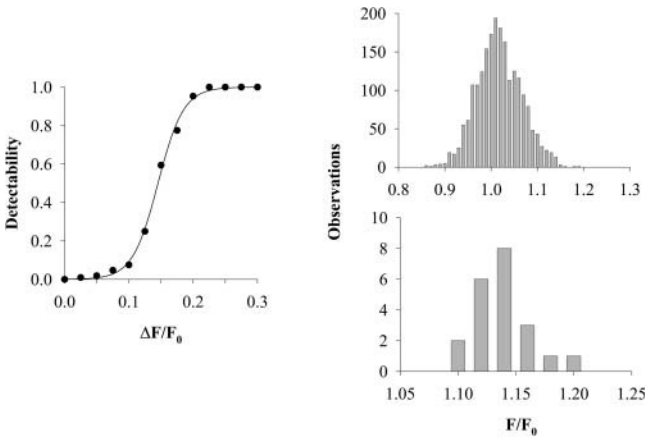

FIGURE 3 Detectability of in-focus Ca^{2+} sparks. (*Left*) Spark detectability determined by feeding test images through the same automated spark detection algorithm. For construction of test images, the average spark in Fig. 2 *B* was variably scaled and randomly embedded in a noise background produced by pixel scrambling of four event-free images. (*Right*) Signal-to-noise characteristics. (*Top*) All-point histogram of $\Delta F/F_0$ from 2100 points in 21 blank traces. (*Bottom*) Histogram of peak $\Delta F/F_0$ in 21 blank traces.

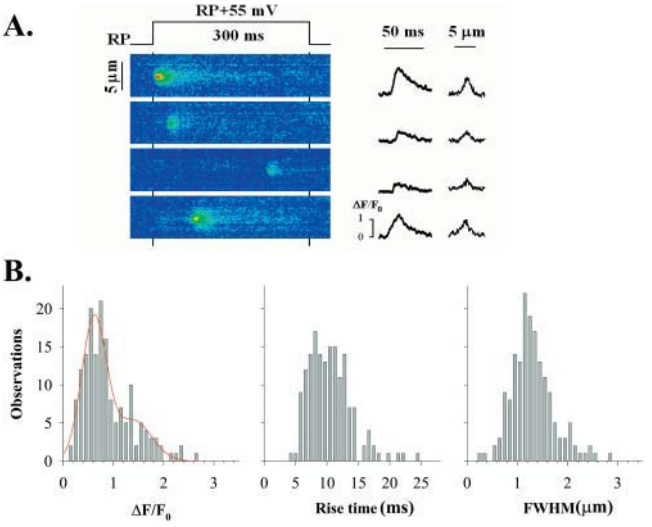

FIGURE 4 Morphometrics of in-focus Ca^{2+} sparks. (*A*) Evoked Ca^{2+} sparks from a representative patch. From left to right, linescan images, local Ca^{2+} transients (spatially averaged over 1.1-μm width), and spatial profiles of the first Ca^{2+} sparks at peak (averaged over seven scans or 5.4 ms). Note the large event-to-event variation and the crisp appearance of sparks regardless of brightness. (*B*) Histograms of spark amplitude (*left*), rise time (*middle*), and FWHM (*right*). The overlay to the amplitude histogram shows the least-square, two-component Gaussian fit of the data, which peaks at 0.67 and 1.45, respectively.

Morphometrics of Ca^{2+} sparks

With the out-of-focus blurring and false detection essentially eliminated, we were set to measure true Ca^{2+} spark morphometrics and population statistics. Fig. 4 *A* shows the results from a representative patch in which Ca^{2+} sparks were evoked stochastically at variable latencies during repeated depolarization to *RP* + 55 mV (−25 mV). Visual examination suggested that Ca^{2+} sparks evoked from the same release unit were not stereotyped; instead, they were highly variable by virtue of brightness and morphology. We characterized Ca^{2+} spark morphometrics by four main parameters, amplitude, rise time, mean or maximal rising rate, and spatial width (full width at half maximum, FWHM) at peak amplitude, which reflect, to the first approximation, the amount of released Ca^{2+}, the release duration (or inversely the rate of spark termination), the magnitude of release flux, and the spatial scope of spark signaling, respectively. We found that the amplitude of in-focus sparks displayed a broad and leftward skewed distribution (Fig. 4 *B*, *left*), in agreement with our previous report (Wang et al., 2001). The overall amplitude histogram was empirically fitted to a bimodal Gaussian function, with a prominent mode at 0.67 ($\Delta F/F_0$ unit) and a second minor mode at 1.45. Of the 166-event data set, the dimmest spark was 0.27, well above

our detection threshold (Fig. 3, *left*), and the brightest one was 2.75. The mean and median spark amplitudes were 0.98 and 0.88, respectively, similar to those reported previously for randomly sampled events (Cannell et al., 1995; Cheng et al., 1993; Lipp and Niggli, 1994; Lopez-Lopez et al., 1995). The similarity of in-focus and randomly sampled sparks in terms of their average amplitudes is somewhat surprising, because one might expect in-focus sparks be brighter than randomly sampled ones. However, this can be explained as the net result of two opposing factors, the absence of out-of-focus events (which tends to increase the average amplitude) and the enhanced detectability for low-amplitude events (which tends to decrease the average amplitude) in this study. Similar to the case with spark amplitude, a large variation was observed for the mean rising rate ($99.1 \pm 62.8\ s^{-1}$, $n = 166$ events). The variations in the amount of Ca^{2+} released and the releasing flux indicate that Ca^{2+} sparks are polymorphic, rather than a stereotyped or all-or-none phenomenon (Bridge et al., 1999; Cannell et al., 1995; Cheng et al., 1993; Lipp and Niggli, 1994; Lopez-Lopez et al., 1995).

As shown in Fig. 4 *B*, *middle*, spark rise time histogram rose steeply at 6 ms (eight scan lines) and then decayed precipitately at 14 ms, with the vast majority (90%) distributed over this narrow time window. Thus, the rise time distribution of in-focus sparks deviates from exponential distributions expected for Markovian channels or channel groups that gate reversibly (Colquhoun and Hawkes, 1995; Wang et al., 2002). This underpins the notion that Ca^{2+} release duration in a spark or the rate of spark termination is tightly regulated by some unknown, thermodynamically irreversible mechanism.

Ca^{2+} sparks sampled at random locations exhibit a broad FWHM distribution with an average value of 2.0 μm (Cannell et al., 1995; Cheng et al., 1993; Lipp and Niggli, 1994; Lopez-Lopez et al., 1995). Yet, models of spark formation often predicted a FWHM around 1.0 μm even after confocal blurring effects were accounted for (Colquhoun and Hawkes, 1995; Pratusevich and Balke, 1996; Smith et al., 1998). Deceptively trivial, this twofold discrepancy in FWHM would translate into an eightfold discrepancy in spatial volume, and it has been difficult to reconcile this ''spark-width paradox'' (Smith et al., 1998), unless a large Ca^{2+} current (20–40 pA) was assumed, which results in gross saturation of the Ca^{2+} indicator and flat-top (''platykurtic'') Ca^{2+} sparks (Izu et al., 2001). The experimental setting permitted us to revisit this important issue by measuring spatial characteristics of in-focus Ca^{2+} sparks. Fig. 4 *A* shows that, whether big or small, in-focus sparks displayed a sharply peaked spatial profile that rapidly decayed at increasing radius, giving no sign of local indicator saturation (at the optical resolution). In the absence of out-of-focus events, the FWHM distribution showed a prominent mode at 1.25 μm, with a greatly reduced dispersion compared to randomly sampled events (Fig. 4 *B*, *right*). The average and median FWHW for in-focus sparks were 1.41 and 1.35 μm, respectively, which is considerably smaller than the reported values. The downwardly revised FWHM, together with the moderate amplitude, would greatly reduce the Ca^{2+} current needed to account for the genesis of Ca^{2+} sparks. The remaining discrepancy between theoretical and observed FWHM, if any, has to be accounted for by reasons other than gross indicator saturation. For instance, regenerative recruitment of adjacent release units (Parker et al., 1996) might explain the platykurtic subpopulation of sparks under some experimental conditions (Izu et al., 2001).

Polymorphism of Ca^{2+} sparks within and among individual release units

There are competing hypotheses as to whether a single RyR (Cheng et al., 1993; Shirokova et al., 1999), the entire RyR release unit (Bers and Fill, 1998; Sobie et al., 2002), or a fraction of RyRs in a unit are activated in a spark (Bridge et al., 1999; Cannell et al., 1995; Cheng et al., 1993; Lipp and Niggli, 1994; Lopez-Lopez et al., 1995; Shirokova et al., 1999; Wang et al., 2001). To this end, analysis of variability of Ca^{2+} sparks evoked from single in-focus release units should be informative. Among 15 events observed in patch [1] in Fig. 5, morphometric measurement revealed a 6.6-fold difference between the brightest and the dimmest spark amplitudes (Fig. 5 *A*, *left*), accompanying a 5.6-fold difference in mean rising rate (Fig. 5 *A*, *right*). Similar results were obtained from three other patches illustrated in Figs. 5 *A*, and diaries of mean and standard deviation in all 20 patches displaying four or more events are shown in Fig. 5 *B*. It is

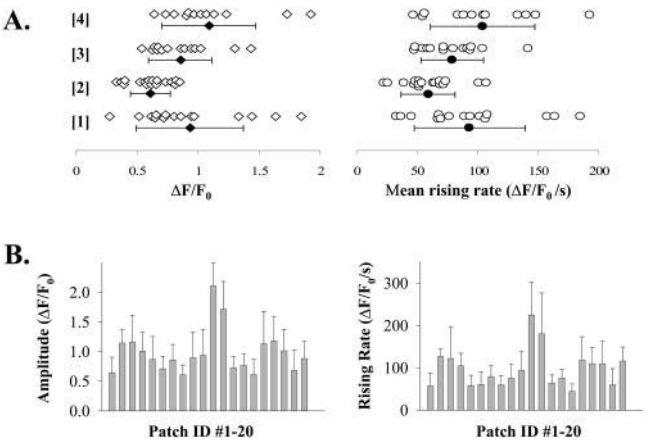

FIGURE 5 Intrinsic variability of Ca^{2+} sparks from individual patches. (*A*) Scatter plots of amplitude (*left*) and mean rising rate (*right*) of Ca^{2+} sparks from four different patches. Small vertical displacements were added to avoid overlapping symbols. The mean ± SD was shown below respective scatter plot. (*B*) Diary of mean ± SD for amplitude (*left*) and mean rising rate (*right*) from individual patches (in the order of data acquisition). Seven patches that displayed three or fewer evoked events were not included. $n =$ 4–17 events in each patch.

noteworthy that there was a significant patch-to-patch variation in spark characteristics. For instance, the average spark amplitudes in patch [2] and [3] of Fig. 5 *A* were 0.61 ± 0.16 ($n = 17$) and 0.86 ± 0.26 ($n = 14$, $p < 0.01$), the mean rising rates were 59.6 ± 22.3 ($n = 17$) and 79.4 ± 25.7 s^{-1} ($n = 14$, $p < 0.05$), respectively. The patch-to-patch variation suggests that cardiac release units are somewhat heterogeneous with respect to organization or operation.

To quantify spark variability within and among release units, we defined variability (ν) as the ratio of standard deviation (SD) and the corresponding mean value. For the pooled population of sparks, the ν was 0.51 for amplitude or 0.63 for mean rising rate; the ν-value within release units (ν_1) was, on average, 0.34 or 0.41 ($n = 20$), and the ν-value among release units (ν_2) was 0.38 or 0.46, for spark amplitude or mean rising rate, respectively. In either case, these ν-values satisfied the relationship $\nu_1 \approx \nu_2$ and $\nu^2 \approx \nu_1^2 + \nu_2^2$. Thus, both intra- and interrelease unit variability contributed equally to the overall spark variability. Since the noise in blank traces was equivalent to 3–5 nM Ca^{2+} fluctuation (at the resting Ca^{2+} level) (Fig. 3, *right*), photon collection noise should account for only a small portion of the observed amplitude variability.

Interrelationship between spark parameters

As shown in Fig. 4 *A*, spark activation was scattered over almost the entire depolarization pulse at ~−25 mV. This provided an opportunity to investigate whether early sparks differ from those activated late into the pulse. Fig. 6, *A* and *B*, show scatter plot of spark amplitude and maximal rising rate as a function of the latency of activation, with overlay of the linear regression lines, respectively. Our data show clearly that spark parameters are stationary during the pulse, independently of the latency of spark production and the time-dependent changes in L-type channel activation.

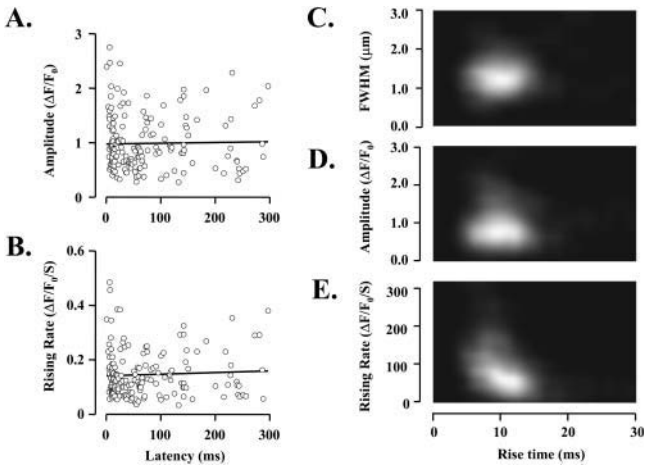

FIGURE 6 Interrelationship between spark parameters. (*A* and *B*) Scatter plot and linear regression of spark amplitude (*A*) or maximal rise rate (*B*) as a function of activation latency (at −25 mV). (*C–E*) Joint histograms of spark rise time and FWHM (*C*), or amplitude (*D*), or mean rising rate (*E*). The brightest part represents 10 or 11 events. The histograms were plotted after interpolation by the cubic convolution method of Park and Schowengerdt (1983).

To determine relationship between different aspects of spark morphometrics, we constructed two-dimensional joint histograms for pairs of spark parameters. In joint histogram of rise time and FWHM, nearly all events were found within a single condensed cluster (Fig. 6 *C*). The joint distribution of rise time and amplitude, however, dispersed substantially along the amplitude dimension (Fig. 6 *D*), evidencing the polymorphic feature of Ca^{2+} sparks. The polymorphism of Ca^{2+} sparks was better shown by the joint histogram for rise time and mean rising rate (Fig. 6 *E*). To quantify the relationship between spark parameters, we calculated the matrix of correlation coefficient. This analysis revealed that the stereotyped spark width displayed little correlation with spark amplitude ($r = 0.17$), rise time ($r = 0.08$), or mean rising rate ($r = 0.14$). Spark amplitude was independent of rise time ($r = 0.07$), but was strongly and positively related to the mean or maximal rising rate ($r = 0.82$ or 0.94, respectively). The lack of correlation between spark amplitude and rise time indicates that polymorphism of Ca^{2+} sparks is not due to variation in the underlying release duration. Rather, the variation in the underlying release flux per se and its strong positive correlation with spark amplitude suggest that a Ca^{2+} spark consists of a variable number of participant RyRs that opened for a relatively stereotyped duration, giving rise to variable spark amplitude.

Furthermore, we uncovered a substantial negative correlation between the release duration and flux (rise time and mean rising rate) ($r = -0.43$), as if a stronger release current terminated the spark sooner. This observation is consistent with previous reports that the rate of termination of spark release flux is directly related to the magnitude of the flux (Lukyanenko et al., 1998; Soeller and Cannell, 2002). Since the opposite is predicted for local CICR among RyRs in a cluster, some intraunit negative feedback mechanism must be at work for spark termination. Taken together, our morphometric data support a model in which cohorts of variable number of RyRs are activated in the genesis of Ca^{2+} sparks, and the ensuing negative feedback, which strength depends on the degree of activation, overrides the positive feedback by CICR to extinguish the ongoing Ca^{2+} spark.

DISCUSSION

Determination of spark morphometrics is fundamental to appraising various biophysical processes involved in spark formation and delimiting the spatial and temporal scope of local Ca^{2+} signaling. By activation and visualization of in-focus Ca^{2+} sparks, we have provided the first accurate measurement of true Ca^{2+} spark morphology, their population statistics, and intra- and interunit variability, as well as correlation between different spark parameters. As com-

pared to previous studies aiming at similar goals (Bridge et al., 1999; Izu et al., 1998; Klein et al., 1999; Rios et al., 2001; Shirokova et al., 1999; Wang et al., 2002), the unique advantages of the current approach include the absence of out-of-focus events, the suppression of positive and negative false detection, and the ability to activate repetitive Ca^{2+} sparks from the same well-defined, in-focus release units. In addition, all experiments were performed with intact cardiac myocytes with normal physiological saline. Under the experimental conditions, we have demonstrated that, despite relatively stereotyped spark rise time and spatial width, Ca^{2+} sparks exhibit large intrinsic variability in rising rate and amplitude, even when they are evoked from the same release units.

Precautions should be taken in the acquisition, analysis, and interpretations of the loose-seal spark data. Since the pipette can only access the LCCs residing on the surface of the cell, the spark data reflect primarily the peripheral excitation-contraction (EC) coupling. To this end, we compared spark activation to T-tubule spike generation (under whole-cell patch-clamp conditions). Our results revealed similar coupling kinetics in either case, suggesting that the peripheral EC coupling is representative of those at the T-tubule sites. Besides, even in the loose-seal configuration, local CICR may sometimes be altered by spontaneous Ω-shaped deformation. We therefore from time to time monitor the seal resistance and membrane boundary to ensure minimal perturbation on the local CICR. Further, we limited the imaging scan time at a given release site such that statistical spark properties did not drift within the sequence of collection (data not shown). These efforts help to minimize possible limitations of the loose-seal method and ensure that the obtained spark data are physiologically relevant.

The polymorphism of Ca^{2+} sparks within and among cardiac release units explains our previous report on a broad modal amplitude distribution for in-focus Ca^{2+} sparks (Wang et al., 2001), but is in apparent contrast with the conclusion by Bridge et al. (1999). Although both studies reported on a modal (rather than monotonic decreasing) spark amplitude distribution, they attributed a large portion of the apparent variability among sparks evoked by action potentials at fixed T-tubule-SR sites to the photon collection noise. In light of the finding that sparks can be both dim and bright, a biased rejection of small-amplitude events amidst noise could have compromised their conclusion. In their histogram analysis of local $[Ca^{2+}]$ at a fixed time after the action potential, the identity of the intermediates (i.e., those between the peaks for baseline and sparks) was uncertain, making it difficult to appraise the true spark variability. Even though sparks of varying amplitude were commonly seen at many T-tubules in their study, it was unclear whether this apparent variability was intrinsic to the spark genesis, because activation of multiple out-of-focus sites could also render large apparent same-site variation. Thus, we believe our observations are consistent with data in the previous study. Other circumventive evidence for polymorphism of Ca^{2+} sparks includes the observation that recurrent sparks at Imperatoxin A-modified sites are highly variable (Terentyev et al., 2002).

The origin of polymorphism has not yet been determined experimentally. In principle, the interrelease unit variability should reflect heterogeneity in the organization or operation of different release units (Franzini-Armstrong et al., 1999). Within individual release units, spark variability may arise from genuine moment-to-moment variation in the recruitment of RyRs. Also, the stochastic nature of the coupling between single LCCs and the abutting RyR array may add variability to sequence of the same-patch events (triggered by different LCCs). Theoretical analysis of a model array of RyRs has suggested a possible spark origin as intraunit mesoscopic Ca^{2+} wave driven by CICR (Stern et al., 1999). To this end, an intriguing possibility might be that the variable spark rising rate may due to simultaneous ignition of more than one focus within a unit: those of fast rising rate and large release current could reflect events of multiple intraunit foci. If this were the case, spark properties might be expected to vary with the probability of LCC and spark activation. Under our experimental conditions, spark activation at ~ -25 mV dispersed widely with varying probability during 300-ms depolarization. However, spark properties including the rising rate do not vary with the latency of spark production. This indicates that polymorphism of Ca^{2+} sparks does not reflect time-dependent changes in LCC and spark activation under current experimental conditions. Future investigation is warranted to delineate the molecular and cellular origin of spark polymorphism.

Irrespective of its origin, polymorphism of Ca^{2+} sparks has multifaceted implications. The large intrinsic variation in Ca^{2+} spark mean rising rate would be difficult to reconcile with any model in which sparks are generated by the entire release unit (Bers and Fill, 1998; Sobie et al., 2002), or a single RyR (Cheng et al., 1993; Shirokova et al., 1999), or any fixed number of RyRs. Instead, it is in favor of the idea that variable cohorts of RyRs in the same unit can be activated in a stochastic, rather than deterministic, manner. If the coupled gating whereby multiple RyRs operate in unison (Marx et al., 2001, 1998) does exist in vivo, our data suggest that the mechanical coupling of RyRs operates over a limited range, and undergoes dynamic reorganization within a unit. Finally, the polymorphism of Ca^{2+} sparks adds an interesting twist to the debate on the molecular nature of Ca^{2+} sparks: a subpopulation of sparks may be genuinely single-channel events. To this end, the presence of very weak in-focus sparks and the existence of a small population of long-lasting, slow-rising events may represent single RyR ''quarks'' (Lipp and Niggli, 1998) or RyR ''sparklets'' (Wang et al., 2001) triggered under physiological conditions. It should be noted that since the number of RyRs participating in an average cardiac spark is estimated to be ~4–6 (Wang et al., 2001), the small-amplitude Gaussian

component shown in Fig. 4 *B* may not correspond to single-RyR events.

With the current 50% event detection level at ~0.15 $\Delta F/F_0$ units, the scarcity of events smaller than 0.30 $\Delta F/F_0$ units suggests that, during microscopic EC coupling, SR Ca^{2+} is released in discrete packets that are resolvable with our current Ca^{2+} imaging capability. Hence, our data support the notion that, albeit polymorphic, Ca^{2+} sparks constitute the elementary events of cardiac EC coupling, and summation of discrete sparks accounts for the totality of SR Ca^{2+} release (Cannell et al., 1995; Cheng et al., 1993; Lipp and Niggli, 1994; Lopez-Lopez et al., 1995). Should subspark events or eventless releases (Lipp and Niggli, 1996, 1998) exist in heart cells, their unitary amplitudes must be below the current detection limit (~0.10 $\Delta F/F_0$ units).

Characterization of spark morphometrics also sheds some new light on possible mechanism that is responsible for the termination of Ca^{2+} sparks. The narrow rise time distribution, in defying of the stochastic law that governs channel gating (Colquhoun and Hawkes, 1995; Wang et al., 2002), strongly suggests that spark termination is under rigorous regulation. The negative correlation between spark rise time and the mean rising time suggests that this regulation is a negative feedback in nature, the strength of which is proportional to the ongoing release flux or the number of activated RyRs. Mechanistically, this could either be a Ca^{2+}-dependent inactivation overriding local CICR (Fabiato, 1985; Sham et al., 1998), or inhibitory regulation of RyRs through depletion of local SR lumenal Ca^{2+} (Terentyev et al., 2002). The manyfold variation in the amplitude (thereby the amount of Ca^{2+} released) of Ca^{2+} sparks from individual release sites argues against local SR Ca^{2+} depletion as the sole or primary determinant of termination of Ca^{2+} sparks, although a modulatory role for SR lumenal Ca^{2+} cannot be excluded (Terentyev et al., 2002). Finally, the inverse relationship between spark rising rate and rise time is in contrast to the observation that, in planar lipid bilayers, coupled RyRs have their open duration prolonged by orders of magnitudes compared to RyRs acting solo (Marx et al., 2001).

In summary, characterization of in-focus Ca^{2+} sparks has revealed both stereotyped and polymorphic spark properties. The newly quantified spark amplitude, rise time, mean rising rate, and full width at half maximum are, on average, 1.0 $\Delta F/F_0$ unit, 10 ms, 100 s^{-1}, and 1.4 μm, respectively, which are independent of the latency of spark production during depolarization. The spark morphometrics, their population statistics and intrinsic variability support a model in which spark activation involves stochastic recruitment of variable number of RyRs in a release unit. With Ca^{2+} release duration being the most tightly regulated spark parameter, termination of Ca^{2+} spark apparently entails a strong negative feedback mechanism. Furthermore, the identification of interrelease unit variability provides a means to appraise heterogeneity among Ca^{2+} release units. The novel approach developed in this and recent studies (Wang et al., 2001) should prove to be crucial in mechanistic studies of microscopic EC coupling in heart and local Ca^{2+} signaling in many types of cells.

We thank Drs. Edward G. Lakatta and Ira R. Josephson for critical reading of this manuscript, and Mark B Cannell for valuable discussion.

This work was supported by Predoctoral Fellowship of the National Institutes of Health Graduate Partnership Program (JXS), National Institute on Aging (Scientific Director's Award in Research), awards by China Ministry of Education (SQW), National Institutes of Health intramural research programs, National Natural Science Foundation of China (TH, HC), and Major State Basic Research Development Program of China (HC).

REFERENCES

Bers, D. M., and M. Fill. 1998. Coordinated feet and the dance of ryanodine receptors. *Science*. 281:790–791.

Bridge, J. H., P. R. Ershler, and M. B. Cannell. 1999. Properties of Ca^{2+} sparks evoked by action potentials in mouse ventricular myocytes. *J. Physiol.* 518:469–478.

Cannell, M., H. Cheng, and W. J. Lederer. 1995. The control of calcium release in heart muscle. *Science*. 268:1045–1050.

Cheng, H., W. J. Lederer, and M. B. Cannell. 1993. Calcium sparks: the elementary events underlying excitation-contraction coupling in heart muscle. *Science*. 262:740–744.

Cheng, H., M. R. Lederer, R. P. Xiao, A. M. Gomez, Y. Y. Zhou, B. Ziman, H. Spurgeon, E. G. Lakatta, and W. J. Lederer. 1996. Excitation-contraction coupling in heart: new insights from Ca^{2+} sparks. *Cell Calcium*. 20:129–140.

Cheng, H., S. L. Song, N. Shirokova, A. Gonzalez, E. G. Lakatta, E. Rios, and M. D. Stern. 1999. Amplitude distribution of calcium sparks in confocal images: theory and studies with an automatic detection method. *Biophys. J.* 76:606–617.

Colquhoun, D., and A. G. Hawkes. 1995. The principles of the stochastic interpretation of ion-channel mechanisms. *In* Single Channel Recording, 2nd ed. B. Sakmann and E. Neher, editors. Plenum Press, New York. 397–482.

Fabiato, A. 1985. Time and calcium dependence of activation and inactivation of calcium-induced release of calcium from the sarcoplasmic reticulum of a skinned canine cardiac Purkinje cell. *J. Gen. Physiol.* 85:247–289.

Franzini-Armstrong, C., F. Protasi, and V. Ramesh. 1999. Shape, size and distribution of Ca^{2+} release units and couplons in skeletal and cardiac muscles. *Biophys. J.* 77:1528–1539.

Guia, A., M. D. Stern, E. G. Lakatta, and I. R. Josephson. 2001. Ion concentration-dependence of rat cardiac unitary L-type calcium channel conductance. *Biophys. J.* 80:2742–2750.

Haak, L. L., L. S. Song, T. F. Molinski, I. N. Pessah, H. Cheng, and J. T. Russell. 2001. Sparks and puffs in oligodendrocyte progenitors: cross talk between ryanodine receptors and inositol trisphosphate receptors. *J. Neurosci.* 21:3860–3870.

Izu, L. T., J. R. Mauban, C. W. Balke, and W. G. Wier. 2001. Large currents generate cardiac Ca^{2+} sparks. *Biophys. J.* 80:88–102.

Izu, L. T., W. G. Wier, and C. W. Balke. 1998. Theoretical analysis of the Ca^{2+} spark amplitude distribution. *Biophys. J.* 75:1144–1162.

Klein, M. G., H. Cheng, L. F. Santana, Y. H. Jiang, W. J. Lederer, and M. F. Schneider. 1996. Two mechanisms of quantized calcium release in skeletal muscle. *Nature*. 379:455–458.

Klein, M. G., A. Lacampagne, and M. F. Schneider. 1999. A repetitive mode of activation of discrete Ca^{2+} release events (Ca^{2+} sparks) in frog skeletal muscle fibres. *J. Physiol.* 515:391–411.

Lipp, P., and E. Niggli. 1994. Modulation of Ca^{2+} release in cultured neonatal rat cardiac myocytes. Insight from subcellular release patterns revealed by confocal microscopy. *Circ. Res.* 74:979–990.

Lipp, P., and E. Niggli. 1996. Submicroscopic calcium signals as fundamental events of excitation-contraction coupling in guinea-pig cardiac myocytes. *J. Physiol.* 492:31–38.

Lipp, P., and E. Niggli. 1998. Fundamental calcium release events revealed by two-photon excitation photolysis of caged calcium in Guinea-pig cardiac myocytes. *J. Physiol.* 508:801–809.

Lopez-Lopez, J. R., P. S. Shacklock, C. W. Balke, and W. G. Wier. 1995. Local calcium transients triggered by single L-type calcium channel currents in cardiac cells. *Science.* 268:1042–1045.

Lukyanenko, V., T. F. Wiesner, and S. Gyorke. 1998. Termination of Ca^{2+} release during Ca^{2+} sparks in rat ventricular myocytes. *J. Physiol.* 507:667–677.

Marx, S. O., J. Gaburjakova, M. Gaburjakova, C. Henrikson, K. Ondrias, and A. R. Marks. 2001. Coupled gating between cardiac calcium release channels (ryanodine receptors). *Circ. Res.* 88:1151–1158.

Marx, S. O., K. Ondrias, and A. R. Marks. 1998. Coupled gating between individual skeletal muscle Ca^{2+} release channels (ryanodine receptors). *Science.* 281:818–821.

Nelson, M. T., H. Cheng, M. Rubart, L. F. Santana, A. D. Bonev, H. J. Knot, and W. J. Lederer. 1995. Relaxation of arterial smooth muscle by calcium sparks. *Science.* 270:633–637.

Park, S., and R. Schowengerdt. 1983. Image reconstruction by parametric cubic convolution. *Comp. Vis. Graph. Image Process.* 23:256–265.

Parker, I, W. J. Zang, and W. G. Wier. 1996. Ca^{2+} sparks involving multiple Ca^{2+} release sites along Z-lines in rat heart cells. *J. Physiol.* 497:31–38.

Pratusevich, V. R., and C. W. Balke. 1996. Factors shaping the confocal image of the calcium spark in cardiac muscle cells. *Biophys. J.* 71:2942–2957.

Rios, E., N. Shirokova, W. G. Kirsch, G. Pizarro, M. D. Stern, H. Cheng, and A. Gonzalez. 2001. A preferred amplitude of calcium sparks in skeletal muscle. *Biophys. J.* 80:169–183.

Sham, J. S., L. S. Song, Y. Chen, L. H. Deng, M. D. Stern, E. G. Lakatta, and H. Cheng. 1998. Termination of Ca^{2+} release by a local inactivation of ryanodine receptors in cardiac myocytes. *Proc. Natl. Acad. Sci. USA.* 95:15096–15101.

Shirokova, N., A. Gonzalez, W. G. Kirsch, E. Rios, G. Pizarro, M. D. Stern, and H. Cheng. 1999. Calcium sparks: release packets of uncertain origin and fundamental role. *J. Gen. Physiol.* 113:377–384.

Smith, G., J. Kiezer, M. D. Stern, W. J. Lederer, and H. Cheng. 1998. A simple numerical model of calcium spark formation and detection in cardiac myocytes. *Biophys. J.* 75:15–32.

Sobie, E. A., K. W. Dilly, J. Dos Santos Cruz, W. J. Lederer, and M. S. Jafri. 2002. Termination of cardiac Ca^{2+} sparks: an investigative mathematical model of calcium-induced calcium release. *Biophys. J.* 83:59–78.

Soeller, C., and M. B. Cannell. 2002. Estimation of the sarcoplasmic reticulum Ca^{2+} release flux underlying Ca^{2+} sparks. *Biophys. J.* 82: 2396–2414.

Song, L. S., S. Q. Wang, R. P. Xiao, H. Spurgeon, E. G. Lakatta, and H. Cheng. 2001. β-adrenergic stimulation synchronizes intracellular Ca^{2+} release during excitation-contraction coupling in cardiac myocytes. *Circ. Res.* 88:794–801.

Stern, M. D., L. S. Song, H. Cheng, J. S. K. Sham, H. T. Yang, K. R. Boheler, and E. Rios. 1999. Local control models of cardiac excitation-contraction coupling: a possible role for allosteric interactions between ryanodine receptors. *J. Gen. Physiol.* 113:469–489.

Terentyev, D., S. Viatchenko-Karpinski, H. H. Valdivia, A. L. Escobar, and S. Gyorke. 2002. Luminal Ca^{2+} controls termination and refractory behavior of Ca^{2+}-induced Ca^{2+} release in cardiac myocytes. *Circ. Res.* 91:414–420.

Tsugorka, A., E. Rios, and L. A. Blatter. 1995. Imaging elementary events of calcium release in skeletal muscle cells. *Science.* 269:1723–1726.

Wang, S. Q., L. S. Song, E. G. Lakatta, and H. Cheng. 2001. Ca^{2+} Signaling between single L-type Ca^{2+} channels and ryanodine receptors in heart cells. *Nature.* 410:592–596.

Wang, S. Q., L. S. Song, L. Xu, G. Messiner, E. Rios, M. D. Stern, and H. Cheng. 2002. Thermodynamically irreversible gating of ryanodine receptors in situ revealed by stereotyped duration of release in Ca^{2+} sparks. *Biophys. J.* 83:242–251.